Acoustic emission measurement in the proof loading of an existing bridge affected by ASR

Yang, Yuguang; Hordijk, Dick; de Boer, A.

DOI
10.1201/9781315375175-146

Publication date
2016

Document Version
Final published version

Published in
Proceedings of the 5th International Symposium on Life-Cycle Civil Engineering

Acoustic emission measurement in the proof loading of an existing bridge affected by ASR

Y. Yang, D.A. Hordijk
Delft University of Technology, Delft, Netherlands

A. de Boer
Ministry of Infrastructure and Environment, Netherlands

ABSTRACT: Proof loading has been considered as an effective approach in the assessment of existing concrete bridges. This paper presents a study of acoustic emission measurement in a proof loading of an ASR affected concrete slab bridge (Zijlweg bridge). Because of the uncertainty on the mechanical properties of the ASR affected concrete. The attenuation contours, the wave speed and the geometry effect were studied before the proof loading. During the proof loading, zonal location based on signal strength was applied to track the cracking active area. In addition, the combination of load ratio and calm ratio was used to assess the damage level caused by proof loading. The study showed that the additional damage caused by proof loading was limited. Besides, the presented approach appears to be a promising tool for proof loading.

1 INTRODUCTION

1.1 *Proof loading of concrete slab bridges*

Assessment of the residual capacity of existing structures has being raised increasing attention in Europe. Many of the existing structures that do not fulfill the requirement of current design codes are of rather complex material properties or boundary conditions. Available theoretical models cannot accurately evaluate their capacities. Proof loading is considered as one of the effective alternatives. The principle of proof loading is to evaluate the capacity of a structure by applying the desired load condition directly. When the structural behavior does not violate the predefined stop criteria, the structure is approved to a corresponding capacity.

In the Netherlands, assessment of concrete slab bridges with proof loading became an interesting option recently. In most cases, the concrete slab bridges are of short span. Thus the design load is relatively small, moderate load level is needed for proof loading. On the other hand, these structures are often vulnerable to shear failure, which is rather difficult to be calculated accurately with the design expression proposed by the present design codes (EN 1992-1-1, 2010, fib, 2012). Consequently, proof loading on the structure becomes a realistic option.

1.2 *AE measurement in proof loading*

As one of the basic principles for proof loading, the loading process should not affect the structural safety. Therefore, the assessment of possible additional damage caused by proof loading becomes essential. However, conventional methods are mostly related to the crack width of structure or the strain of the reinforcing steel (DAfStb, 2000). Such measurements are dependent on the choice of monitoring locations. Besides, they can only cover a relatively small area of the target structure.

On the other hand, Acoustic Emission (AE) measurement has been applied in monitoring the cracking behavior of concrete specimens in laboratory for years. Review of relevant researches can be found in (Ohtsu et al., 2007, Carpinteri and Lacidogna, 2008). In principle, the acoustic emission measurement technology monitors the acoustic activities of the structural member during the loading and unloading processes. The AE wave signals usually emerge rapidly and randomly in time. Therefore they are more suitable to be discretised from running waves into separate activities. These separate activities are defined as hits. The source of such a hit is called event. The user predefines a threshold of voltage level. Only when the AE signal's amplitude is higher than the threshold, that part of the signal is defined as active.

Because of the uncertainty of the wave transfer function caused by the complex geometry and material properties in an existing structure, the conventional approaches based on source location based measurements need further calibration on large-scale concrete structures. To do so, consistent experimental results on structures with similar conditions are of interest.

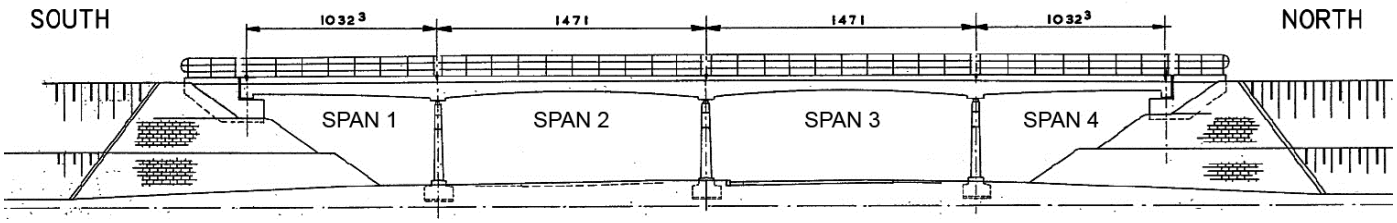

Figure 2 Side view of Zijlweg bridge.

This paper presents the AE measurement on the proof loading on an ASR (alkali silica reaction) affected existing bridge: Zijlweg bridge in the Netherlands, see Figure 1. Because of the expansion effect caused by the swelling of the ASR product (CSH gel), a large amount of cracks were observed on the bottom surface of the deck before the test. The AE signals measured during the test are studied briefly in this paper. Recommendations on the execution of AE measurements and assessment of the measured results are given in the paper.

2 PROOF LOADING ON ZIJLWEG BRIDGE

2.1 *Introduction*

The Zijlweg bridge (viaduct) is a four span concrete slab bridge across the highway A59 in the southern part of the Netherlands. The bridge was constructed in 1965 and Alkaline Silica Reaction (ASR) was found since 1997. The traffic on the bridge was restricted since then. From 2003, the Ministry of Infrastructure and Environment in the Netherlands (Rijkswaterstaat) decided to apply an hourly monitoring on this bridge regarding temperature, moisture and expansion of the bridge deck. After more than 10 years of monitoring, it was found that the expansion of the deck caused by ASR is stabilized. In 2015, it was decided to proof loading the bridge in order to assess the residual capacity of the bridge. If the capacity of the bridge is proved to be sufficient, it is possible to remove the restriction of the traffic.

Figure 1. Zijlweg bridge (viaduct) in the highway A59 in the province Brabant, the Netherlands.

2.2 *Conditions of the tested span*

For safety reason, the proof loading was carried out on one of the side spans, span 4 in Figure 2. The length of span 4 is 10.32 m. The width of the deck is 6.60 m, with a 4.00 m carriageway, see Figure 3. The limited total width results one driving lane on the bridge with two sidewalks. The slab thickness of the deck varies from 0.55 m next to the edge cross beam, to 0.85 m close to the intermediate cross beam. In the width direction, the deck thickness at the edge is slightly lifted at the carriageway.

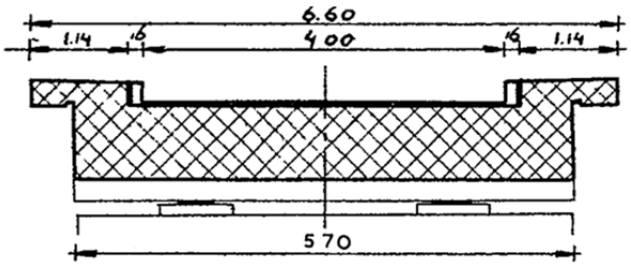

Figure 3. Cross section of the deck of Zijlweg bridge.

The concrete quality of the bridge deck was determined previously from cylinder specimens by (Witteveen+Bos, 2014). It turned out that the ASR did not significantly affect the concrete compressive strength. The measured strength is $f_{cm,cube}$ = 44.4 MPa, and f_{ck} = 24.5 MPa. Since the bridge was constructed in the 60s, smooth rebar with low yielding strength was employed as reinforcement.

Before the test, a visual inspection was carried out. Based on that, the crack pattern on the bottom surface of the bridge deck was marked, see Figure 8.

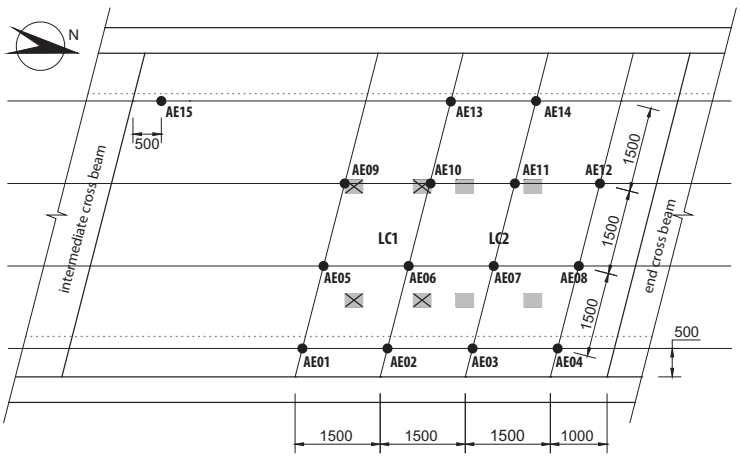

Figure 4. Locations of the wheel print in comparison with AE sensors.

2.3 *Proof loading*

During the proof loading, the flexural capacity (load case 1) and the shear capacity (load case 2) of the bridge deck were assessed. Two axel loads with wheel prints of 230×300 mm^2 were used to represent the Eurocode prescribed load model LM1. The size of the wheel print is based the recommendation given by Rijkswatestraat (Rijkswaterstaat, 2013). The axel loads were placed at the locations that generate the maximum cross sectional action / capacity ratio. The locations of the wheel prints are indicated in Figure 4. A detailed description the proof loading process is reported in (Koekkoek et al., 2015).

In both load cases, several load steps were defined in the loading procedure. After a load step was reached, the deck was unloaded to a minimum load level. The highest load step was designed to be slightly higher than the Eurocode design load for additional safety when it can be reached.

2.4 *AE measurement during proof loading*

In total 15 AE sensors were installed on the bottom surface of the bridge deck. Their locations formed a grid aligned with the edges of the deck. The distance between two neighbour sensors in one direction of the grid is 1.5 m. A reference sensor AE15 is located at the far end of the bridge deck. The locations and the numbers of the sensors are indicated in Figure 4. The grid was further evaluated on site taking into account the attenuation property of the concrete deck in section 3.1.

The AE sensors that are employed in the proof load tests are R6I-AST, the transfer function of which is given in Figure 5. Its response frequency is up to 100 kHz. During the test, the low frequency components (< 20 kHz) were filtered.

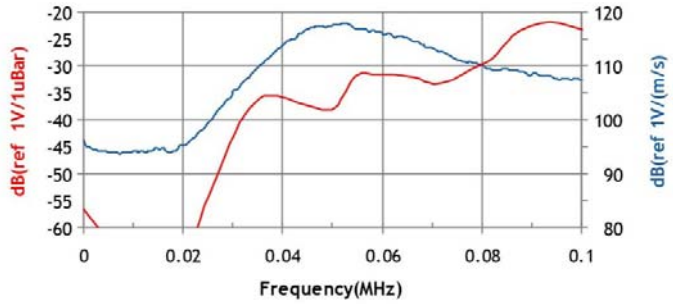

Figure 5. Transfer function of R6I-AST (Physical Acoustics, 2016).

3 STUDY OF AE TRANSFER PROPERTIES

3.1 *Introduction*

The swelling of the CSH gel generated by ASR in concrete may result in degradation of concrete compressive strength, elastic modules, and other mechanical propertied (Jones and Clark, 1998, Giaccio et al., 2008). In addition, the expansion of concrete in combination with the confinement by the longitudinal reinforcement results in cracking along the reinforcement directions. As shown in Figure 8, in addition to the bending cracks in the transverse direction, cracks along the longitudinal direction of the bridge deck were observed before the test. They locate mostly around the part of the bridge deck close to the side carriageway. All these aspects might affect the wave transfer properties in the deck. Besides, the surfaces of the structure and the existing cracks might influence the reflection of the AE signals. Thus further study on the transfer functions of the parameters of a hit was necessary before the execution of the proof loading. The two main aspects that were studied before the proof loading were: the attenuation properties around the sensors and the average wave speed.

3.2 *Attenuation properties*

The attenuation of the amplitude of a surface wave signal is related to the elastic modules of the material. It is typically measured by assessing the peak amplitude of a hit generated by the breaking of a pencil lead, also name by pencil break test (PBT) at different distances away from an AE sensor. The amplitude reduction percent – distance relationship is expressed by an attenuation curve. For uncracked concrete, the attenuation curve is homogeneous in all directions, thus the attenuation curve measured in one direction is representative for all directions. In the case of Zijlweg bridge, the influence of the existing cracks on the attenuation curve has to be taken into account. The prescribed AE sensor grid should be close enough to monitor the hits from the sources located within the grid. This means that the peak amplitude of an effective AE hit will not be lower than the threshold when it arrives the sensor.

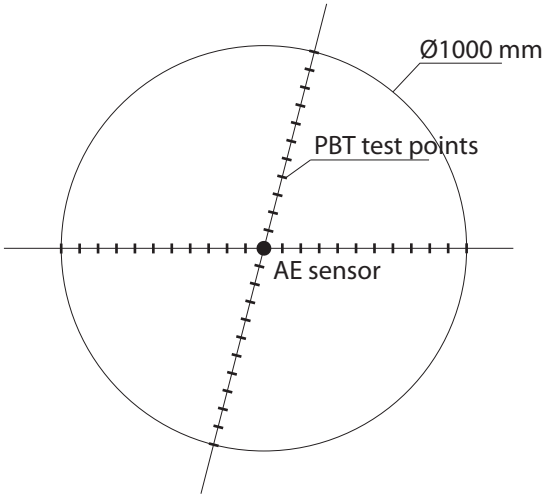

Figure 6. Pencil break test (PBT) position around an AE sensor.

The attenuation curves of five sensors were measured on site, namely AE03, AE05, AE06, AE07 and AE08. These sensors are located at the part of the deck with higher bending moment, and many cracks, thus they are representative to the whole sensor grid. For each sensor, the attenuation

curve was measured in four directions, two in the longitudinal direction of the bridge, and the other two in the transverse direction. In each direction, 10 PBT was carried out when the test location was accessible. The first test position was at 100 mm from the target sensor. The following ones were spaced at 100 mm. An indication of the positions of the PBT positions of one sensor is given in Figure 6.

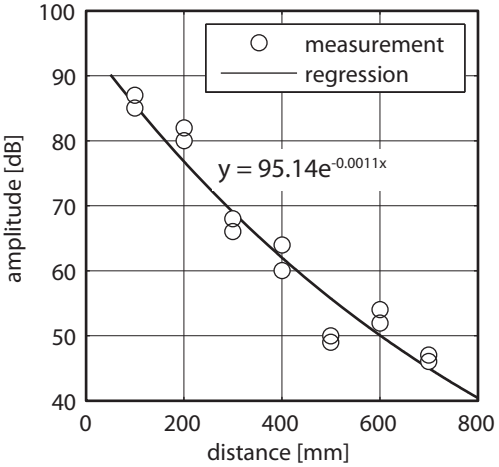

Figure 7. Attenuation curve of AE05 in the western direction

At each test point, the PBT were repeated twice, thus maximum 80 PBT were executed per AE sensor. The final attenuation curve in one direction is the exponential regression of the measured peak amplitudes from the PBT. As an example, the measured amplitudes of AE05 in the western direction and the resultant regression curve are given in Figure 7. As shown in Figure 8, despite the fact that many cracks were observed in the vicinity of AE05, the attenuation of the amplitude of the hits from PBT was still quite consistent. It turns out to be possible to use a continuous function to represent the attenuation relationship, even when cracks are present. Although the curve fitting process smoothed the possible sudden change of the attenuation curve, the global trend can still be represented.

With the regression curves in the four directions determined, the values of the amplitudes at the PBT testing points were recalculated. The four amplitude values with the same distance to the AE sensor are then used to linear interpolate a distribution of amplitude along the entire perimeter. In this way an attenuation contour plot is determined around the measured AE sensors. In Figure 8, the attenuation contour of AE03, AE05, AE06, AE07 and AE08 are ploted. As comparison, the crack pattern of the bridge deck is included as well.

It has to be remarked that in the laboratory, the peak amplitude determined by PBT at 100 mm from the AE sensors on is typically about 85 – 90 dB. However, the same test yielded only 77 dB signals on site. It turns out that the rough concrete surface on the bridge deck has a non-negligible effect on the amplitude of the AE hits. In order to take that into account, it is decided not to put the percentage of the amplitude over the maximum one, but to use the absolute value in Figure 8. The peak amplitude of a PBT is representative to the hits that are generated by the cracking of concrete. Thus the contour of the 45 dB of an AE sensor based on PBT can be used to represent the boundary of the sensitivity of the sensor regarding the cracking activity. During the proof

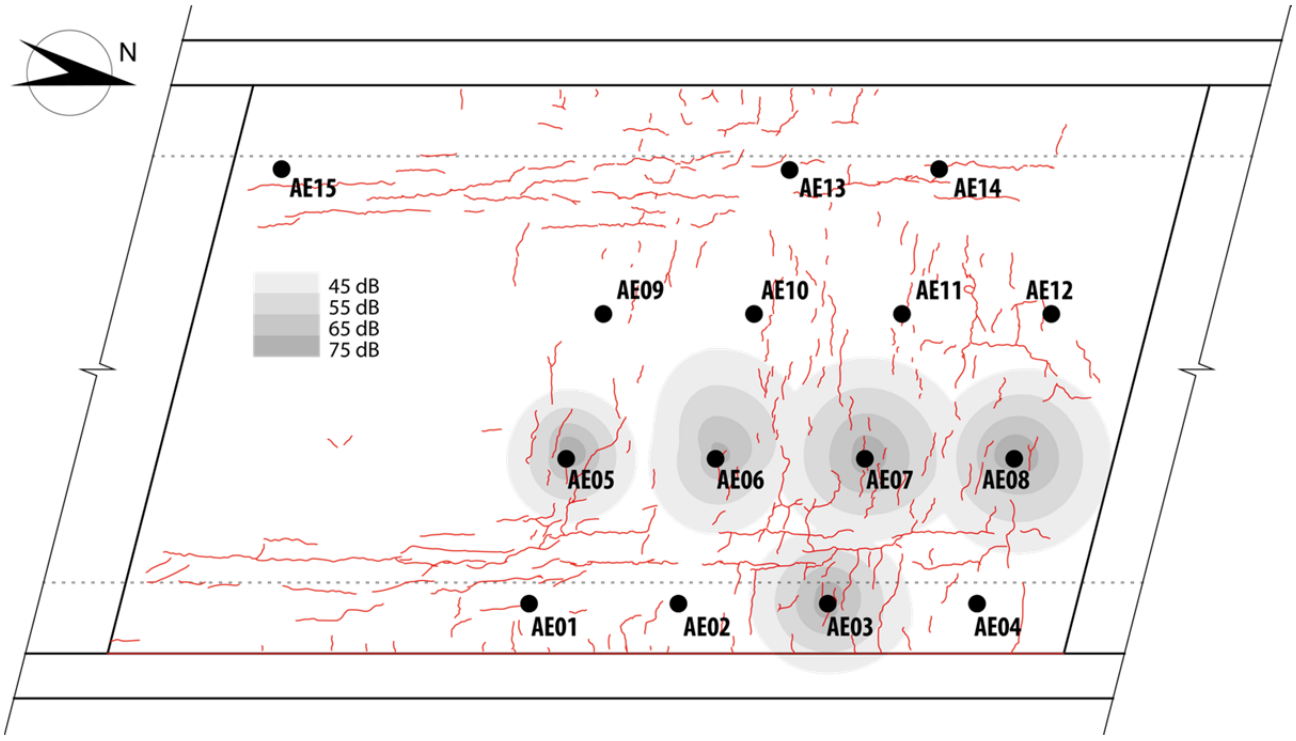

Figure 8. Attenuation contour of sensor AE03 - AE08 in comparison with crack pattern before proof loading

loading, the threshold of the AE sensors was 45 dB.

The comparison between the measured AE attenuation contour and the crack pattern shows that the two parameters are clearly related. At the part of the deck with fewer cracks or with the cracks propagates towards the sensor, the attenuation contour extended further, vice versa, see AE06 and AE03. Despite the influence of the cracks to the attenuation contour, the 45 dB contours of the measured 5 AE sensors covered the majority part of the deck between the sensors. Since the measured AE sensors are mostly located at heavily cracked part of the deck, it is safe to assume that the AE sensors are close enough for the proof loading.

3.3 *Wave speed*

In addition to the attenuation contours, the average surface wave speed was also investigated on site. Considering that the PBT could not generate sufficient peak amplitude due to the rough surface, the test was based on the hits generated by a strong hit with a steel hammer. The closer distance between the test location and one of the sensors was 500 mm. The average wave speed is calculated as follows:

$$v = \frac{t_1 - t_2}{d_1 - d_2}$$

With t_i the arriving time of sensor i and d_i the distance between sensor i and the test location.

The wave speed between a sensor pair was determined by at least two tests. For the same sensor pair, the resultant wave speed turns out to be stable between tests. The mean value of the surface wave speed based the executed test is 1708 m/s. However, a relatively large scatter is found between the sensor pairs at different locations, the COV of the wave speeds is 30%. The variation of the wave speed at different locations results in a wrong estimation of the distance between the signal source and the sensor, thus a wrong estimation of the location of the signal source with the conventional triangulation approach. During the proof loading, when the crack width increases with the load level, the variation of wave speed could be higher. Therefore, it is more practical to use the so-called zonal location approach, which divides the monitoring structure by several zones with an AE sensor in the center of the zone. The cracking activities in a given zone are represented by the monitored AE activity of the sensor.

3.4 *Wave transfer study*

Before the proof loading was executed, several preliminary tests were carried out in order to further investigate the characteristics of the AE signals from different other sources.

The first part of the test was to evaluate the effect of activity of workers on the bridge deck to the AE measurement. After the AE sensors was installed and calibrated, a fellow was asked to walk from the north end of the tested span to the south. The test was repeated for 6 times. The person walked with two different manners: walking with normal steps or trying to make additional slips at every step, and at three parts of the driving lane: the middle, the west side and the east side. The study showed that the friction between the shoe and the bridge surface is already sufficient to generate recognizable AE hits. When additional slips were made during walking, the amount of hits was enormously increased. Thus during the proof load, any unnecessary activities above the bridge deck should be forbidden. Nevertheless, the hits that are caused by the friction on the deck are mostly located in a very narrow band in the signal strength – duration diagram (Figure 9), which makes it possible to filter out such type of hits.

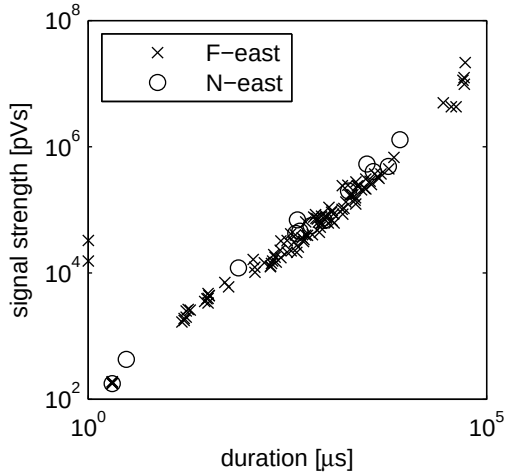

Figure 9. Duration vs. Signal strength of AE hits generated by walking above the bridge deck.

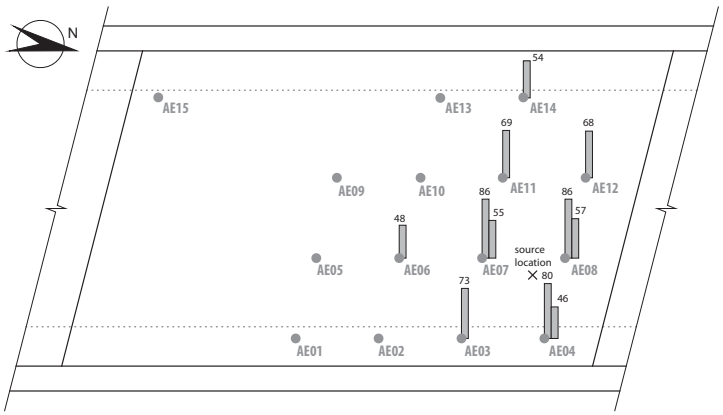

Figure 10. Distribution of the measured amplitude from a hammer hit.

In the second part of the study, the AE hits generated by hammering on the top surface of the bridge deck were studied. The study was to evaluate the influence of the deck geometry on the signal transfer. As an example, one of the hammering tests with its location indicated in Figure 10 is discussed. The recorded peak amplitudes from the sensor grid are indicated in the same figure. It turned out that due to the reflection of the wave at the top surfaces,

a single event could indeed result in two hits, see AE07, AE08 and AE04 in Figure 10. The amplitude of the second hit received by these sensors is significantly reduced. Since the amplitude is calculated with log scale, summation of the parameter is not possible.

On the other hand, the signal strength seems to be a better parameter to represent the location of the cracking activity. The definition of signal strength is the integral of the rectified acoustic emission signal voltage within the duration of the burst signal. It represents the energy of an AE hit. In the study of the hits generated by hammers, only the sensors that are very close to the signal source would receive hits with large signal strength. The signal strength of those that are further away from the source location dropped very fast. As an example, the signal strengths of the entire AE sensor grid during seven hammering tests are plotted in Figure 11. Where, the hits are always clustered after the corresponding hammer hit. Therefore they can be easily linked to a hammer hit. The figure shows that in most cases, the hit recorded by the sensor closest to the hammer hit location was with significantly larger signal strength than the other sensors. It implies that since the signal strength of an event decreases fast with the increase of the distance, the accumulative hit rate only rises when the cracking activity is close the sensor. Therefore, the accumulative signal strength rate vs. time can be used as a parameter to represent the cracking activities in the zonal location approach.

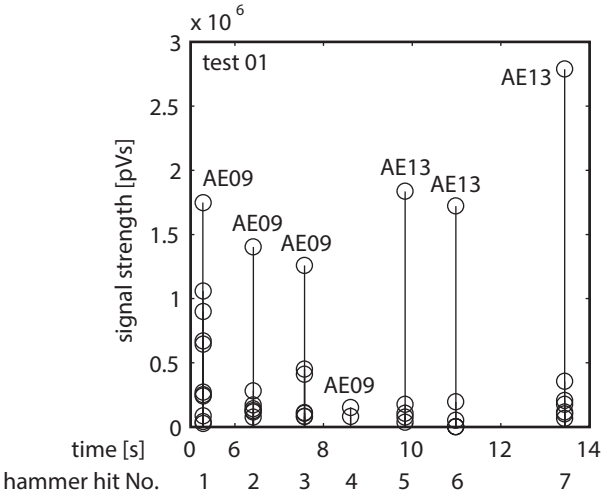

Figure 11. Signal strength of the hits recorded during the hammering tests

4 ACOUSTIC EMISSION DURING PROOF LOADING

4.1 *Introduction*

The proof loading of Zijlweg bridge included two load cases. They were designed to assess the bending and shear capacity of the bridge deck respectively. In this paper, only the measurement results of load case 1 (bending load case) is presented. The maximum load level applied in this load case was higher than the other one. A detailed analysis of the AE measurement result from both load cases is reported in (Yang and Hordijk, 2015).

The loading procedure of load case 1 is shown in Figure 12. In the loading procedure, 11 load steps (LS) with more or less 5 load levels can be distinguished. For the convenience of further study, the load steps are numbered in Figure 12. The 5 load levels are listed in Table 1. As comparison, the equivalent load level with respect to the different safety levels of Eurocode and the requirement of Rijkswaterstaat are given as well. Table 1 shows that from LS2 on, the maximum bending moment was already larger than the moment generated by Eurocode SLS load. At the maximum load step, the applied load was 73 kN higher than that generated by the Eurocode ULS load.

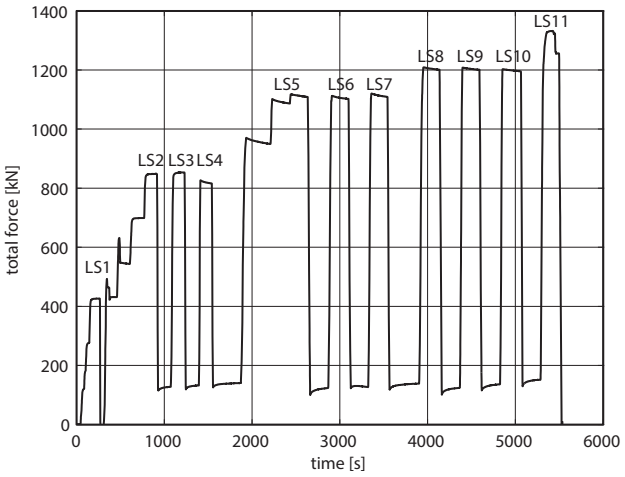

Figure 12. Loading program of LC1.

Table 1. Comparison of the load level required by design codes and the applied load step levels.

Safety level of the design codes	***P* [kN]**	***Load step***	***P* [kN]**
EC ULS	1259	11	1332
RBK Design	1257	8	1209
RBK Reconstruction	1091	5	1118
RBK Usage	1050	2	848
RBK Disapproval	1049	1	426
EC SLS	815		

4.2 *Zonal source location*

Based on the linear elastic FEM analysis performed prior to the proof loading, the AE sensors were classified according to the bending moment at their locations, see Figure 13. The sensors located at positions with larger bending moment are of higher importance.

The inactive sensors: AE01, AE04, AE08, AE12, AE14 and AE15 are not taken into account in the analysis. The maximum hit per second recorded by these sensors were less than 50 hits/sec, while for the active sensors the peak hit rate can be more than 500 hits/sec.

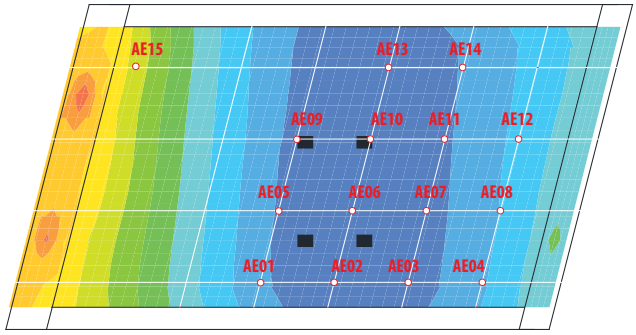

Figure 13. Moment M_{xx} distribution of the deck under LC1 in comparison with AE sensor locations.

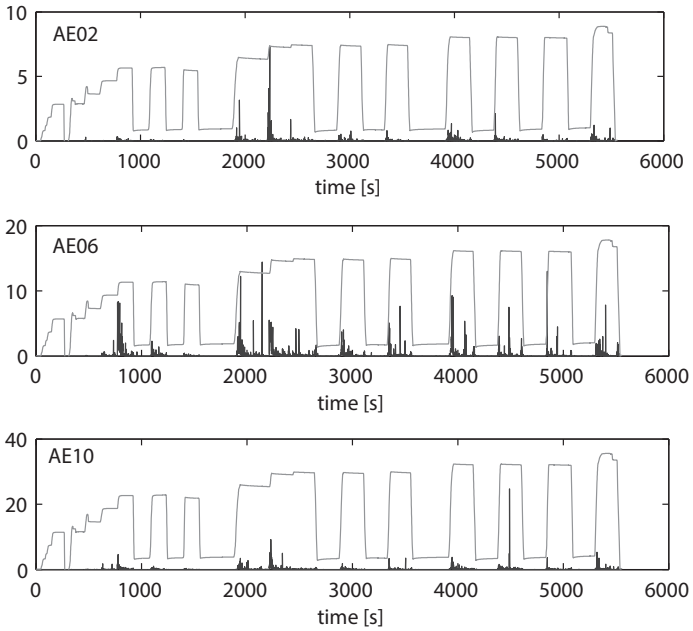

Figure 14. Cumulative signal strength [μVs] per second against time per sensor.

Table 2. Active AE sensors at different load levels

Load level	*Active AE sensor No.*
426 kN	N.A.
848 kN	AE06
1118 kN	AE02 AE06 AE09 AE10 AE11 AE13*
1206 kN	AE03 AE06 AE07 AE10 AE05* AE09*
1332 kN	AE06 AE07 AE09

*only active at the second load cycle.

Take AE02, AE06 and AE10 as example, the cumulative signal strength rate (cumulative signal strength per second) is plotted against time in Figure 14. The loading scheme of LC1 is plotted in the same figure. This assumed that he AE hits were mainly caused by the cracking activities in the concrete deck. When the cumulative signal strength ratio of 5 μVs/s is set as a threshold. Figure 14 shows that the cracking activity started at the maximum load level of LS2 in the vicinity of AE06. The cracking active area extended to AE02 and AE10 when LS5 was reached. While the sensor AE10 only became active at LS9, which was the second time the load level reached about 1200 kN. Similarly, the activities of all the AE sensors at the 5 load levels are listed in Table 2. In general, the development of the cracking activities extended from the location with the maximum bending moment (AE) towards the supports and the sides according to the signal strength approach. That was in line with the estimation given by the FEM analysis.

In the second load case, because of the heavy load of the first load case, much less signal strength rate was monitored among the AE sensors.

4.3 *Damage assessment*

With the locations of the damages determined, the level of the damage has to be evaluated as well. The load ratio and calm ratios proposed by (Ohtsu et al., 2002, Ohtsu et al., 2010) was adapted to assess the potential additional damage caused by the proof loading. The definition of the two terms are given as follows:

$$\text{load ratio} = \frac{\text{load at the onset of AE activity in the subsequent load cycle}}{\text{the previous maximum load}}$$

$$\text{calm ratio} = \frac{\text{the number of cumulative AE activity under unloading}}{\text{total AE activity during the whole load cycle}}$$

In general, the load ratio represents the stability of the crack propagation. A lower load ratio implies unstable crack development. The calm ratio indicates the crack opening. A higher calm ratio means bigger crack widths. The closing of the opened cracks causes more AE hits. These two parameters only compares information collected within the same loading procedure, rather than using absolute criteria. That minimizes the uncertainties among the different material and structural geometries of different structures.

This approach has been adapted previously in the structural test on an existing bridge Ruytenschildt bridge in 2014 (Yang, 2014). In that test, the structure was loaded until the yielding of longitudinal reinforcement. In the Ruytenschildt bridge test, the relationship between the load – calm ratio and the damage level of the bridge based on other measurements was assessed. The thresholds of the ratios proposed by Ohtsu have been calibrated based on the test. The modified damage scale is listed in Table 5

Table 3. Load ratio of AE01-AE14 calculated from load step 5 to load step 11.

sensor No.	*LS5*	*LS6*	*LS7*	*LS8*	*LS9*	*LS10*	*LS11*
01	1.14	1.00	1.00	1.05	1.00	1.00	1.07
02	0.98	0.67	0.80	0.61	0.45	0.46	0.65
03	0.98	0.60	0.83	0.84	0.72	0.51	0.83
04	1.00	1.00	1.00	1.00	1.00	1.00	1.00
05	0.83	0.60	0.80	0.81	0.72	0.85	0.86
06	0.60	0.27	0.39	0.43	0.29	0.40	0.50

07	0.80	0.57	0.53	0.65	0.50	0.46	0.72
08	1.14	1.00	1.00	1.06	1.00	0.99	1.00
09	0.92	0.77	0.77	0.89	0.76	0.85	0.90
10	0.88	0.53	0.66	0.52	0.50	0.51	0.65
11	0.97	0.77	0.87	0.89	0.72	0.77	0.86
12	1.14	1.00	1.00	1.08	1.00	0.97	0.22
13	0.92	0.77	0.73	0.81	0.67	0.72	0.86
14	1.11	0.99	0.98	1.01	1.00	0.99	1.01

Table 4. Calm ratio of AE01-AE14 calculated from load step 5 to load step 11.

sensor No.	*LS5*	*LS6*	*LS7*	*LS8*	*LS9*	*LS10*	*LS11*
01	0.00	0.13	0.00	0.04	0.00	0.00	0.00
02	0.04	0.06	0.06	0.14	0.20	0.22	0.24
03	0.03	0.03	0.09	0.05	0.06	0.06	0.11
04	0.17	N.A.	0.00	0.00	0.00	0.00	0.00
05	0.03	0.04	0.06	0.03	0.06	0.05	0.13
06	0.10	0.16	0.24	0.27	0.28	0.29	0.33
07	0.04	0.06	0.06	0.07	0.10	0.08	0.16
08	0.01	0.08	0.15	0.00	0.05	0.00	0.13
09	0.02	0.03	0.06	0.07	0.16	0.14	0.15
10	0.03	0.05	0.10	0.08	0.12	0.10	0.16
11	0.02	0.12	0.03	0.03	0.05	0.03	0.09
12	0.01	0.00	0.33	0.00	0.00	0.43	0.27
13	0.01	0.05	0.08	0.05	0.05	0.06	0.14
14	0.01	0.00	0.07	0.01	0.03	0.03	0.20

In Table 3 and Table 4, the corresponding load/calm ratios of AE01 to AE14 are given based on the calculation of LS5 to LS11. According to Table 2, only after LS5, the cracking activity started to be active in most AE sensors. The comparison of the load – calm ratios of the sensors listed in Table 3 and Table 4 shows that the most damaged part of the deck is at the area close to AE06. Although AE 12 locates at higher damage scale as well, since the total hits recorded by that sensor was less than 60, it is not taken into account.

Table 5. Definition of damage scale based on Ruytenschildt bridge test (Yang, 2014).

Load ratio	*Calm ratio*	*Damage level*
<0.5	>0.4	Heavily damaged
<0.5	0.2-0.4	Moderate damage
<0.5	0.0-0.2	Light damage
0.5-0.9	0.3-1.0	Light damage
0.5-0.9	0.0-0.3	Slight damage
>0.9	-	No damage

The load – calm ratio coordinate calculated in each load step can be plotted to represent the damage level. As an example, the values at LS11 are plotted in Figure 15. In addition, a damage scale calibrated by the previous study (Ruytenschildt Bridge) is given in Table 5. Figure 15 shows that the additional cracking was still at a moderate level even at the last load step, although in that load level the maximum bending moment in the deck was already higher than that can be generated by the ULS load according to Eurocode. That is in line with the conclusion made by the study of the other parameters in (Koekkoek et al., 2015). Since the concrete strength was not affected by ASR, it turns out that the scale developed from structures with normal concrete can be applied on the ASR affected deck as well.

Similarly the load ratio – calm ratio of load case 2 showed even less damage according to the same scale.

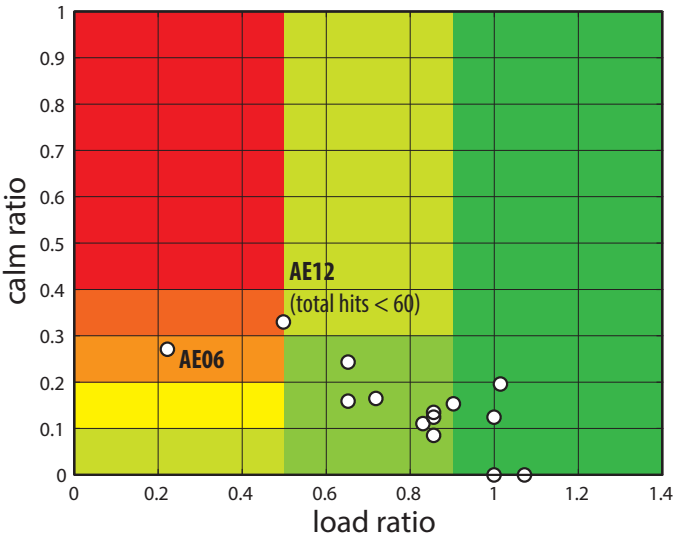

Figure 15. Load ratio - calm ratio of AE01-AE14 at load step 11.

5 CONCLUSIONS

In this paper, the AE measurement during the proof loading of an ASR affected concrete slab bridge deck is studied.

Preliminary study suggested that the friction between the shoes of a worker and the deck surface would generate recognizable AE hits. Therefore during the proof loading, any unnecessary activities on the bridge deck should be forbidden.

The attenuation contour of the AE sensors, that locate at the heavily loaded part of the slab, was measured. The measurement confirmed that the crack distribution indeed affects the attenuation of the amplitude of an AE hit. Nevertheless, the arrangement of the AE sensors grid was still sufficient to catch the AE hits with the peak amplitude as a pencil break test.

The measurement showed a relative large variation of the wave speed at difference locations. It suggests that accurate source location based on triangulation is not possible. Zonal location is therefore recommended.

The influence by the geometry of the bridge deck was assessed by hammer hit. It turned out that the reflection of the deck surface might result in additional hits. However, the signal strength of the hit reduced quickly with the increase of traveling distance. Thus, the AE sensors, which are closer to the source location, recorded the hits with significant larger signal strength. Therefore the signal strength is a more robust indication that can be used in the zonal location approach.

The zonal location was applied by checking the signal strength – time relationship of the AE sensor. The peaks in the signal strength – time graph of an AE sensor were used to indicate the cracking activities close to that AE sensor. The results compare well with the expectation based on the moment distribution calculated with FEM.

Regarding the additional damage level of the cracking active area, the load – calm ratios were used in the evaluations. Although the maximum load level at the last load cycle was higher than the highest safety level required by Eurocode, there was still very limited additional damage level. The conclusion was confirmed by the other measurement results in (Koekkoek et al., 2015).

ACKNOWLEDGEMENTS

The authors wish to express their gratitude and sincere appreciation to the Province of Friesland, the Dutch Ministry of Infrastructure and the Environment (Rijkswaterstaat), STW and InfraQuest for financing or supporting this research work.

REFERENCES

CARPINTERI, A. & LACIDOGNA, G. 2008. *Acoustic emission and critical phenomena: from structural mechanics to geophysics*, CRC Press.

DAFSTB 2000. DAfStb-Richtlinie - Belastungsversuche an Betonbauwerken.

EN 1992-1-1 2010. NEN-EN 1992-1-1 Design of Concrete Structures: General Rules and Rules for Buildings.

FIB 2012. fib Model Code for Concrete Structures 2010. Lausanne: Ernst & Sohn.

GIACCIO, G., ZERBINO, R., PONCE, J. & BATIC, O. 2008. Mechanical behavior of concretes damaged by alkali-silica reaction. *Cement and Concrete Research,* 38**,** 993-1004.

JONES, A. & CLARK, L. 1998. The effects of ASR on the properties of concrete and the implications for assessment. *Engineering Structures,* 20**,** 785-791.

KOEKKOEK, R., LANTSOGHT, E. O. L. & HORDIJK, D. A. 2015. Proof loading of the ASR-affected viaduct Zijlweg in highway A59. Delft: Delft University of Technology.

OHTSU, M., ISODA, T. & TOMODA, Y. 2007. Acoustic emission techniques standardized for concrete structures. *Journal of Acoustic Emission,* 25**,** 21-32.

OHTSU, M., SHIOTANI, T., SHIGEISHI, M., KAMADA, T., YUYAMA, S., WATANABE, T., SUZUKI, T., VAN MIER, J., VOGEL, T. & GROSSE, C. 2010. Recommendation of RILEM TC 212-ACD: acousticemission and related NDE techniques for crack detectionand damage evaluation in concrete. Test method for damage qualification of reinforced concrete beams by acousticemission. *Materials and Structures,* 43**,** 1183-1186.

OHTSU, M., UCHIDA, M., OKAMOTO, T. & YUYAMA, S. 2002. Damage assessment of reinforced concrete beams qualified by acoustic emission. *ACI Structural Journal,* 99**,** 411-417.

PHYSICAL ACOUSTICS 2016. Product datasheet of R6I-AST sensor.

RIJKSWATERSTAAT 2013. Richtlijnen Beoordeling Kunstwerken, Beoordeling van de constructieve veiligheid van een bestaand kunstwerk bij verbouw, gebruik en afkeur.

WITTEVEEN+BOS 2014. Materiaalonderzoek Bruggen, zaaknummer 31084913: 44G-113-01 - Ongelijkvloerse kruising rijksweg - Zijlweg (Zijlweg). Deventer.

YANG, Y. 2014. Acoustic Emission Measurement and Analysis on Ruytenschildbrug.

YANG, Y. & HORDIJK, D. A. 2015. Acoustic Emission Measurement and Analysis on Zijlwegbrug.